Phase-ordering kinetics of one-dimensional nonconserved scalar systems

A. D. Rutenberg* and A. J. Bray†
Theoretical Physics Group, Department of Physics and Astronomy, The University of Manchester, M13 9PL, United Kingdom
(Received 15 April 1994)

We consider the phase-ordering kinetics of one-dimensional scalar systems. For attractive long-range ($r^{-(1+\sigma)}$) interactions with $\sigma > 0$, "energy-scaling" arguments predict a growth law of the average domain size $L \sim t^{1/(1+\sigma)}$ for all $\sigma > 0$. Numerical results for $\sigma = 0.5$, 1.0, and 1.5 demonstrate both scaling and the predicted growth laws. For purely short-range interactions, an approach of Nagai and Kawasaki [Physica A **134**, 483 (1986)] is asymptotically exact. For this case, the equal-time correlations scale, but the time-derivative correlations break scaling. The short-range solution also applies to systems with long-range interactions when $\sigma \to \infty$, and in that limit the amplitude of the growth law is exactly calculated.

PACS number(s): 64.60.Cn, 64.60.My

I. INTRODUCTION

The quench of a system from a disordered phase to an ordered phase is a nonequilibrium process in which energy is dissipated and any topological defects are eliminated. Typically, the system develops a scaling structure, with a single time-dependent length scale, as the growing broken-symmetry phases compete to select the ordered phase [1]. In this paper we discuss nonconserved one-dimensional (1D) scalar systems, where the competing phases are domains of uniform magnetization and the topological defects are domain walls. We limit our discussion to the late stages of phase ordering, when the domains are much larger than the interface width and the scaling structure, if any, has been established. The phase-ordering dynamics is driven by interactions between domains, rather than by the curvature of domain walls which drives the dynamics of short-range systems in higher dimensions [2]. For short-range 1D systems this interaction is through the exponential tail of the domain-wall profile [3]. For long-range systems, the domains have a direct $r^{-(1+\sigma)}$ interaction.

Following work in dimensions greater than one [4–6], there has been recent interest in 1D systems with attractive long-range interactions. This paper follows up a broader treatment that determined growth laws for a wide variety of scaling systems, including 1D systems with $0 < \sigma < 1$ [7]. Lee and Cardy [8] found analytic and numerical indications of scaling violations and anomalous growth laws for $0 < \sigma \leq 1$, in addition to results consistent with scaling for $\sigma > 1$. This motivated us to extend their numerical studies for systems with $\sigma = 0.5$, 1.0, and 1.5, and to extend our theoretical treatment to all $\sigma > 0$ (Sec. II). We find that larger systems than those studied by Lee and Cardy exhibit both scaling and our predicted growth laws (Sec. II B).

Short-range 1D scalar systems have been studied both numerically [9] and experimentally [10]. Nagai and coworkers have presented a solution assuming uncorrelated domain sizes [11,12]. We rederive their solution with a simplified approach, and show that it is asymptotically exact for systems with purely short-range interactions, and also for systems with long-range interactions in the limit $\sigma \to \infty$ (Sec. III).

A generic energy functional for a 1D system with a scalar order parameter $\phi(x)$ and short-range interactions is

$$H[\phi] = \int dx \, \left[(d\phi/dx)^2 + V(\phi)\right] \, , \tag{1.1}$$

where $V(\phi)$ is a double well potential such as

$$V(\phi) = (\phi^2 - 1)^2. \tag{1.2}$$

We restrict our attention to a potential with symmetric quadratic minima [13]. We can also add long-range attractive interactions,

$$H_{\rm LR} = \int dx \int dr \frac{[\phi(x+r) - \phi(x)]^2}{r^{1+\sigma}}$$
$$\simeq A_\sigma L_\infty \int dk k^\sigma \phi_k \phi_{-k} \tag{1.3}$$

where L_∞ is the system size and we take $\sigma > 0$ for a well defined thermodynamic limit. The long-range interactions dominate the 1D dynamics when they exist, so we have ignored the short-range component of (1.3) for $\sigma \geq 2$.

After a temperature quench into the ordered phase, the equation of motion for the ordering kinetics for nonconserved systems with purely dissipative dynamics is [14]

*Electronic address: mbctpan@hpc.ph.man.ac.uk
†Electronic address: bray@v2.ph.man.ac.uk.

$$\partial_t \phi = -\delta H/\delta\phi. \tag{1.4}$$

For short-range systems, and long-range systems with $\sigma > 1$ [15], there is an ordered phase only at $T = 0$. We restrict ourselves to $T = 0$, with no thermal noise, for *all* cases. For systems with $\sigma \leq 1$, our results will be valid throughout the low-temperature phase since temperature is an "irrelevant variable" in the ordering process [16]. For $\sigma > 1$, and for short-range systems, our results are restricted to the $T = 0$ dynamics (1.4) above, and do not apply to kinetic Ising or continuum diffusion models which have a residual $T = 0$ noise [17]. This allows us to study the nontrivial effects of interactions between domain walls in the phase ordering of these systems.

II. LONG-RANGE ATTRACTIVE INTERACTIONS

We first treat systems with long-range attractive interactions of the form (1.3). As was shown by Lee and Cardy for Ising spins [8], the dynamics of the system is captured by the motion of the domain walls. Consider two sharp domain walls of the same sign at r_i and r_j, as shown in Fig. 1. Their interaction energy E_{ij} is the part of $H_{\rm LR}$ that depends on their separation:

$$E_{ij} = \begin{cases} -(1-\sigma)^{-1}|r_j - r_i|^{1-\sigma}, & \sigma \neq 1 \\ -\ln|r_j - r_i|, & \sigma = 1 \end{cases} \tag{2.1}$$

where we have scaled out a factor of $8/\sigma$. Domains of opposite sign introduce an overall -1 factor to the energy. This interaction energy leads to a force

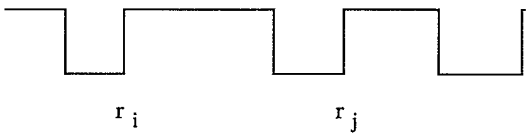

FIG. 1. A schematic representation of the 1D scalar system with domains of $\phi = \pm 1$ shown. The domain walls at r_i and r_j are "positive," and the sign of domain walls alternate along the system. Domain walls of the same sign repel each other, while those of opposite sign attract each other. The dynamics for long-range interactions are described by these sharp Ising-like walls, as is discussed in text.

$$\begin{aligned} F_{ij} &= -\partial E_{ij}/\partial r_j \\ &= \pm l^{-\sigma}, \end{aligned} \tag{2.2}$$

where $l = |r_j - r_i|$ and the force is repulsive between walls of the same sign and attractive between walls of the opposite sign. The domain-wall velocity is proportional to the summed pairwise forces acting on it [18]:

$$\dot{r_i} = \sum_j{}' F_{ij}. \tag{2.3}$$

When adjacent domain walls meet, they annihilate — this drives the nonequilibrium coarsening process. We use the domain-wall dynamics described by Eqs. (2.2) and (2.3) unless specifically noted.

This domain-wall dynamics also holds with the soft potential $V(\phi)$ in (1.2). Fixing the domain wall positions $\{r_i\}$, we use the quasistatic solution of (1.4) expressed in real space:

$$\begin{aligned} 0 &\approx \delta H/\delta\phi \\ &= \partial_x^2\phi - 4\phi(\phi^2-1) + \int_{-\infty}^{\infty} dx' \left[\phi(x') - \phi(x)\right]/|x'-x|^{1+\sigma} \\ &\simeq \phi(x)\left\{-4\left[\phi(x)^2 - 1\right] - 2\sum_{n=0}^{\infty}\left[\int_{r_{i-2n-1}}^{r_{i-2n}} dx'/|x'-x|^{1+\sigma} + \int_{r_{i+2n+1}}^{r_{i+2n+2}} dx'/|x'-x|^{1+\sigma}\right]\right\}, \end{aligned} \tag{2.4}$$

where $x \in (r_i, r_{i+1})$. We use the saturated values $\phi \approx \pm 1$ within the integral, so that the integrals are restricted to phases with $\phi(x') = -\phi(x)$. We also assume that x is far from all domain walls, so that we neglect $\partial_x^2\phi$. This leads to $\phi(x) = \pm[1 - p(x)]$ with

$$p(x) \simeq \frac{1}{4\sigma}\sum_{m=0}^{\infty}(-1)^m\{|x - r_{i-m}|^{-\sigma} + |x - r_{i+1+m}|^{-\sigma}\} \tag{2.5}$$

at large distances from other domain walls (compare [6]). The force corrections due to the asymptotic profile can be easily estimated by the energy per unit length of adding to the ends of the power-law profile between two defects as they move apart. From the potential term in (1.1), $V(\phi) = (\phi^2-1)^2 \sim l^{-2\sigma}$, where the defects are a distance l apart. From the gradient squared term, the effective force is $l^{-2-2\sigma}$, which at late times is always much less than from the local potential. Since we are assuming a quasistatic configuration, the change in energy due to the long-range interactions is of the order of that due to the potential term, so is also $l^{-2\sigma}$. These corrections are negligible in comparison to the $l^{-\sigma}$ interactions of "sharp" domain walls (2.2), which we use without loss of generality.

A. "Energy-scaling" theory for growth laws

We predict the growth law of the characteristic length $L(t)$ for scaling systems by considering the energetics of the system [7]. The scaling behavior, or dependence on the length scale, of the energy density is described by the long-range interactions (1.3):

$$\epsilon \sim \int dk k^{\sigma} \langle \phi_k \phi_{-k} \rangle, \tag{2.6}$$

where the angle brackets indicate an average over initial conditions. We independently calculate the rate of energy-density dissipation by integrating the dissipation in each Fourier mode and using the dynamics (1.4) expressed in momentum space:

$$\begin{aligned} d\epsilon/dt &= \int dk \langle (\delta H/\delta \phi_k) \partial_t \phi_k \rangle \\ &= -\int dk \, \langle \partial_t \phi_k \partial_t \phi_{-k} \rangle \, . \end{aligned} \tag{2.7}$$

We use the equal-time correlation function $S(k,t) \equiv \langle \phi_k \phi_{-k} \rangle$ to determine the energy density, and the time-derivative correlation function $T(k,t) \equiv \langle \partial_t \phi_k \partial_t \phi_{-k} \rangle$ to determine the rate of energy-density dissipation.

If we assume scaling—that the correlations are described by one time-dependent length scale $L(t)$ but not by any microscopic scales—then dimensional analysis determines the structure function:

$$S(k,t) = L(t)\, g(kL(t)), \tag{2.8}$$

where the scaling function $g(x)$ has no time dependence. This is also known as the dynamic scaling hypothesis [19]. We apply the same scaling hypothesis to the two-time correlation function: $S(k,t,t') \equiv \langle \phi_k(t) \phi_{-k}(t') \rangle = k^{-1} \tilde{g}(kL(t), kL(t'), t/t')$. This leads to a scaling form for the time-derivative correlation function:

$$\begin{aligned} \langle \partial_t \phi_k \partial_t \phi_{-k} \rangle &= \partial_t \partial_{t'} |_{t=t'} S(k,t,t') \\ &= (\dot{L}/L)^2 L \tilde{g}_{xy}(kL) + t^{-2} L \tilde{g}_{zz}(kL) \qquad (2.9) \\ &\simeq (\dot{L}/L)^2 L h(kL), \qquad (2.10) \end{aligned}$$

where $\tilde{g}_{xy}$, $\tilde{g}_{zz}$, and h are new equal-time scaling functions. For power-law growth, with or without logarithmic factors, the $\tilde{g}_{zz}$ contribution does not dominate at late times and can be adsorbed into h.

If the energy integrals (2.6) and (2.7) are convergent then we use the scaling forms and change variables to get the L and $\dot{L}$ dependence. Certainly, the integrals are convergent for $kL \ll 1$ if the thermodynamic limit exists. However, the integrals may diverge for $kL \gg 1$. For $S(k,t)$, that limit is given by Porod's law [20], in which the structure at $kL \gg 1$ is proportional to the wall density $\rho_{\rm wall} \sim L^{-1}$,

$$S(k,t) \sim L^{-1} k^{-2} \, , \quad kL \gg 1. \tag{2.11}$$

With this and the scaling form (2.8) we determine the energy density (2.6):

$$\epsilon \sim \begin{cases} L^{-1} \xi^{1-\sigma} \, , & \sigma > 1 \\ L^{-1} \ln (L/\xi) \, , & \sigma = 1 \\ L^{-\sigma} \, , & \sigma < 1. \end{cases} \tag{2.12}$$

For $\sigma > 1$ the integral diverges for $kL \gg 1$ and the energy density is proportional to the domain-wall density, $\rho_{\rm wall} \sim L^{-1}$; for $\sigma = 1$ the logarithmic divergence of the integral indicates that structure on all scales contributes to the energy density; while for $\sigma < 1$ the integral converges and the energy is dominated by the long-range interaction between domains.

The *interaction* energy density $\epsilon_{\rm int}$ of domains at the characteristic scale is the convergent $kL \approx 1$ part of the energy integral. This energy density of interaction is what drives the motion of well separated domain walls:

$$\epsilon_{\rm int} \sim L^{-\sigma}. \tag{2.13}$$

To determine the growth law, we only need the time derivative of $\epsilon_{\rm int}$, which comes from domain walls moving at the characteristic velocity $\dot{L}$. Near a particular domain wall the order parameter comoves with the domain wall:

$$\partial_t \phi = -v \partial \phi / \partial x. \tag{2.14}$$

The contribution of these slowly moving domain walls in momentum space is

$$\begin{aligned} \langle \partial_t \phi_k \partial_t \phi_{-k} \rangle_{\rm int} &\sim \dot{L}^2 k^2 \langle \phi_k \phi_{-k} \rangle \\ &\sim \dot{L}^2 / L, \qquad kL \gg 1 \end{aligned} \tag{2.15}$$

where we use Porod's law to obtain the second line. While this expression satisfies the scaling form (2.10), it is *not* the full time-derivative correlation function, merely the part that contributes to the dissipation of the interaction energy $\epsilon_{\rm int}$. We use this contribution in (2.7) to find

$$d\epsilon_{\rm int}/dt \sim \xi^{-1} \dot{L}^2 / L. \tag{2.16}$$

The integral diverges for $kL \gg 1$, but the divergence reflects the internal structure of the domain walls, rather than small separations with respect to $L(t)$. We compare the rate of energy-density dissipation to the time derivative of (2.13) to obtain $\dot{L} \sim L^{-\sigma}$, which determines the growth law:

$$L(t) \sim t^{1/(1+\sigma)}, \tag{2.17}$$

for all $\sigma > 0$.

We check the consistency of this approach by calculating the full $d\epsilon/dt$. This is easily done in real space, where from (2.7) we have

$$\begin{aligned} d\epsilon/dt &= -L_{\infty}^{-1} \int dx \langle \partial_t \phi(x) \partial_t \phi(x) \rangle \\ &\sim L^{-1} \langle v^2 \rangle, \end{aligned} \tag{2.18}$$

where we have used (2.14) to obtain the second line. The result is the density of domain walls, $\rho_{\rm wall} \sim L^{-1}$, times the average square velocity. Either $\langle v^2 \rangle = \dot{L}^2$ and the energy density is the same as $\epsilon_{\rm int}$, or the energy is dominated by the domain-wall energy and the energy dissipation is dominated by rapidly annihilating domain walls.

For domain sizes $l \ll L$, the force due to nearest neighbors will set the scale of the net force on a domain wall, so from (2.2)

$$|v(l)| \approx \beta l^{-\sigma}, \qquad l \ll L \tag{2.19}$$

where the constant prefactor β, where $0 < \beta \leq 1$, proves

sufficient to parametrize any shielding due to other domain walls. If $n_t(l)$ is the number distribution of domain sizes, so that $n_t(l)\delta l$ is the number of domains of sizes in the interval $[l, l+\delta l]$, then the number flux of collapsing domains is given by $j(l) = n_t(l)\,[-2|v(l)|]$ for $l \ll L$. The factor of 2 follows since the collapse rate of a small domain is twice the speed of each of its walls. When a domain collapses its domain walls vanish, merging the two adjacent domains. Hence every domain that collapses decreases the total number of domains by 2. Matching $2j(\xi)$ to the rate of change of domain number gives $2j(\xi,t) = \partial_t N = -\dot{L}L_\infty/L^2$, where $N = L_\infty/L = \int_\xi^\infty dl n_t(l)$. Since domain walls annihilate at a constant rate over time scales much less than $L/\dot{L}$, the domain-wall flux is constant for scales $l \ll L$: $j(l) \approx j(\xi)$. This leads to

$$n_t(l) \approx \frac{N}{4\beta L}\dot{L}l^\sigma, \qquad l \ll L \tag{2.20}$$

where $\beta = 1$ if no shielding of small collapsing domains occurs.

With (2.19) and (2.20) we determine the contribution of domains of scale $l \ll L$ to the average square velocity:

$$\langle v^2\rangle_{small} = \frac{\int_\xi^L dl v^2(l) n_t(l)}{\int_\xi^L dl n_t(l)}$$

$$\sim \dot{L}L^{-1}\int_\xi^L dl\, l^{-\sigma}$$

$$\sim \begin{cases} \xi^{1-\sigma}\dot{L}L^{-1}, & \sigma > 1 \\ \dot{L}L^{-1}\ln(L/\xi), & \sigma = 1 \\ \dot{L}L^{-\sigma}, & \sigma < 1. \end{cases} \tag{2.21}$$

For $\sigma < 1$ small domains do not dominate the average and, since $\dot{L} \sim L^{-\sigma}$, we have $\langle v^2\rangle \sim \dot{L}^2$. Indeed, for this case $\epsilon \sim \epsilon_{\rm int}$, and the energetics is controlled by domains at the characteristic scale. For $\sigma \geq 1$, the energy-density dissipation, calculated with (2.18) and (2.21), is consistent with (2.12). However, the energy-density dissipation is dominated by small annihilating domains and does not determine the growth law of the average domain size, for which we have used $\epsilon_{\rm int}$.

We have numerically studied the average square velocity of domain walls, as well as the average velocity. In Fig. 2 we show $\langle v^2\rangle/\dot{L}^2$ and $\langle|v|\rangle/\dot{L}$ vs time. The scaled velocity is approximately constant away from early-time transients and late-time small-number effects. Indeed, a similar analysis to that above shows $\langle|v|\rangle \sim \dot{L}$ for all $\sigma > 0$. The average square velocity scales well for $\sigma = 0.5$. However, for $\sigma = 1.0$ and 1.5, $\langle v^2\rangle$ is much larger than $\dot{L}^2$—corresponding to the dominance of small rapidly annihilating domains for $\sigma \geq 1$. While sparse statistics for extremely small domains leads to sporadic undercounting of $\langle v^2\rangle$ for $\sigma \geq 1$, the scaled square velocity for $\sigma = 1.5$ agrees with $\langle v^2\rangle/\dot{L}^2 \sim (L\dot{L})^{-1} \sim t^{1/3}$, which is shown by the straight line.

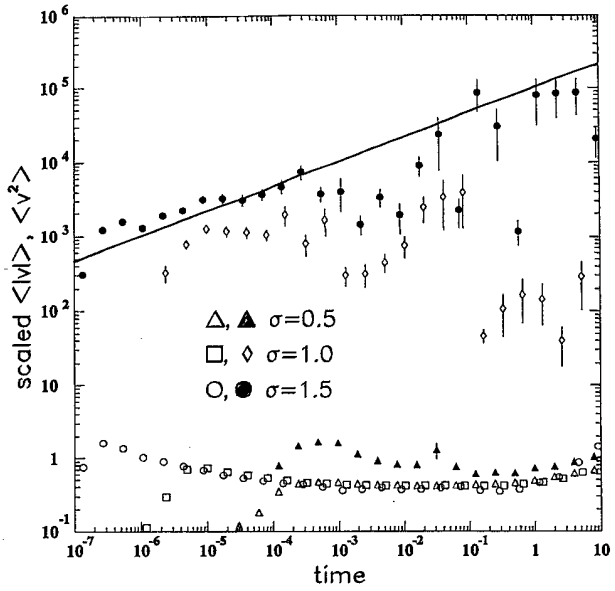

FIG. 2. The bottom plots show simulation results of the scaled average domain-wall velocity $\langle|v|\rangle t^{\sigma/(1+\sigma)}$ vs time for $\sigma = 0.5$, 1.0, and 1.5 with open triangles, squares, and circles, respectively. The upper plots show the scaled square velocity, $\langle v^2\rangle t^{2\sigma/(1+\sigma)}$, vs time with the filled triangles, open diamonds, and filled circles. The dynamics used are given by Eqs. (2.2) and (2.3). Also shown, for comparison, is the $t^{1/3}$ line expected for the scaled square velocity with $\sigma = 1.5$. The systems have periodic boundary conditions, a *fixed* time step, and start with 3200, 1600, and 800 domain walls for $\sigma = 0.5$, 1.0, and 1.5 respectively. Note that the statistical errors shown are not independent.

B. Simulations

To check these growth laws and the scaling of the correlation functions, we perform computer simulations for $\sigma = 0.5$, 1, and 1.5. These are the cases considered by Lee and Cardy [8], and our treatment is motivated by theirs. We simulate the evolution of systems with sharp domain walls of alternating sign which annihilate when they meet. These domain walls are treated as particles. They interact with long-range forces, $f(l) = \pm l^{-\sigma}$, where l is the domain-wall separation. The force is repulsive or attractive for like or unlike domain walls, respectively.

We first measure the number of domain walls $N(t)$ as a function of time, starting from a fixed number placed randomly [21], and continuing until none remain. With a domain-wall velocity proportional to the net force (2.3), we use a simple Euler update for each domain-wall location, $\Delta r_i = \dot{r}_i \Delta t$. Only the early-time behavior depends on the size and nature of the time step Δt, if Δt is small enough. We use a time step proportional to the time ($\Delta t = t/20$), which for power-law growth results in a fixed minimum *scaled* domain size that annihilates in one time step [22],

$$l_{min}/L \propto (\Delta t/t)^{1/(1+\sigma)}. \tag{2.22}$$

The choice of boundary condition only affects the late-

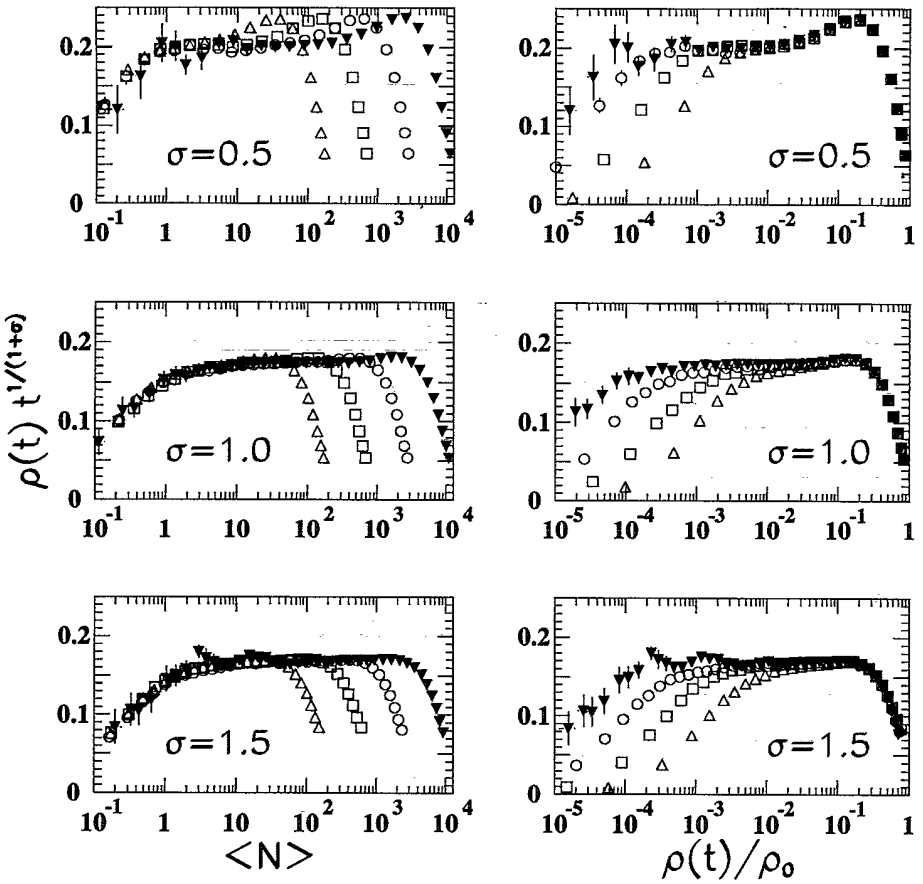

FIG. 3. Φ, the ratio of the measured to expected density (2.23), plotted vs the average number of domain walls [$\langle N\rangle = L_\infty/L(t)$] on the left and vs the ratio of measured to initial density [$\rho(t)/\rho_0$] on the right. The data are for systems starting with 200, 800, 3200, and 12 800 domain walls for open triangles, squares, circles, and filled triangles, respectively. All of the systems have free boundary conditions and an initial random placement of domain walls. Since $\rho(t)/\rho_0 = \langle N\rangle/N(0)$, the two plots collapse either the early- or the late-time behavior.

time results. We use free boundary conditions [23] for which small-number effects are not seen until the average number of domain walls $\langle N\rangle \lesssim 1$, i.e., when most systems have fully ordered. We average over at least a thousand independent runs for most systems, and over at least 50 runs for the largest system size with 12 800 initial domain walls.

We expect the domain size $L(t)$, which is the inverse of the average domain-wall density $\rho(t) = \langle N\rangle/L_\infty$, to have our predicted growth law $L(t) = t^{1/(1+\sigma)}/\Phi^*(\sigma)$. The ratio of the average domain-wall density to the predicted, $\rho(t)t^{1/(1+\sigma)}$ up to the amplitude factor, should be a scaling function of dimensionless combinations of lengths:

$$\rho(t)t^{1/(1+\sigma)} = \Phi\left[\rho(t)/\rho_0, 1/(\rho(t)L_\infty)\right], \qquad (2.23)$$

where ρ_0 is the initial density. In Fig. 3 we plot, for various σ, the scaling function Φ as a function of the average number of domain walls, $\langle N\rangle = \rho(t)L_\infty$, on the left and of $\rho(t)/\rho_0$ on the right. We see an early-time transient [i.e., $\rho_0/\rho(t)$ of order 1] which is independent of the system size, and a small-number regime ($\langle N\rangle \lesssim 1$) at late times which is independent of the initial density [21]. At intermediate times the scaling function is constant, $\Phi = \Phi^*(\sigma) = \Phi[0,0]$, independent of both the initial density and the system size. This indicates a scaling regime, growing with system size, that confirms our predicted growth law $L(t) = t^{1/(1+\sigma)}/\Phi^*(\sigma)$. In Table I we plot the amplitude $\Phi^*(\sigma)$, and also the fixed-point amplitude used by Lee and Cardy, $g_R^*(\sigma) = \Phi^*(\sigma)\,[2(1+\sigma)]^{1/(1+\sigma)}$ [8]. We include the exact amplitude for $\sigma \to \infty$ that we derive in Sec. III [see Eq. (3.12)].

In Fig. 4, we plot Φ vs $\langle N\rangle$ with two different boundary conditions and $\sigma = 0.5$. The scaling regime is of different size in the two systems, but the scaling value $\Phi^*(\sigma)$ is unchanged. The difference is only in the small-number regime ($N \lesssim 20$). We note that systems with periodic boundary conditions and fewer than 800 initial domain walls, as studied by Lee and Cardy for $\sigma = 0.5$ [8], do not probe the scaling regime. We find the expected scaling growth law, $L \sim t^{2/3}$ for $\sigma = 0.5$, in contrast to their numerical results.

The ratio of the measured energy density, $\epsilon(t)$, to the predicted, ϵ (2.12), should be a new scaling function of

TABLE I. The scaling amplitudes of the growth law [see Eq. (2.23)], where $g_R^*(\sigma) = \Phi^*(\sigma)\,[2(1+\sigma)]^{1/(1+\sigma)}$ [8]. These amplitudes are for the dynamics specified in Eqs. (2.2) and (2.3).

σ	$\Phi^*(\sigma)$	$g_R^*(\sigma)$
0.5	0.200 ± 0.005	0.42 ± 0.01
0.75	0.180 ± 0.005	0.37 ± 0.01
1.0	0.175 ± 0.005	0.35 ± 0.01
1.5	0.170 ± 0.005	0.32 ± 0.01
∞	$e^{-\gamma_E}/2 \simeq 0.28$	$e^{-\gamma_E}/2 \simeq 0.28$

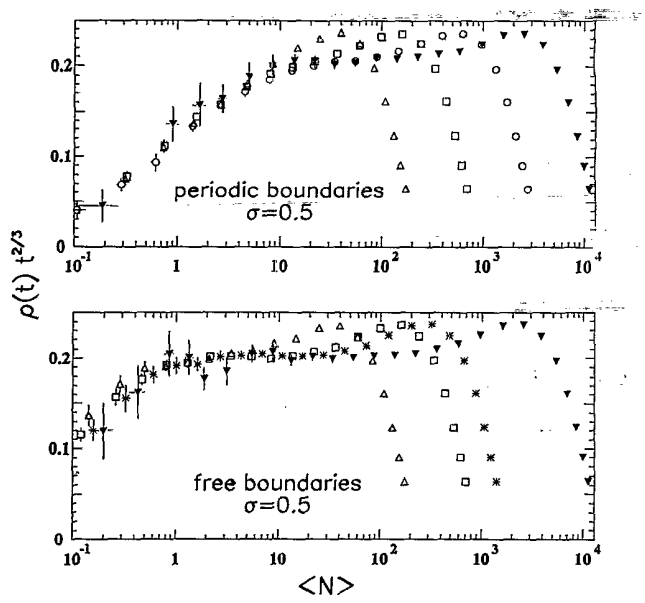

FIG. 4. The ratio of the measured to expected density up to a constant factor (2.23) plotted vs the number of domain walls for $\sigma = 0.5$. The top figure corresponds to periodic boundary conditions with no cutoff to the force law, while the bottom figure corresponds to free boundary conditions. The point types are the same as for Fig. 3, with stars corresponding to systems starting with 1600 domain walls.

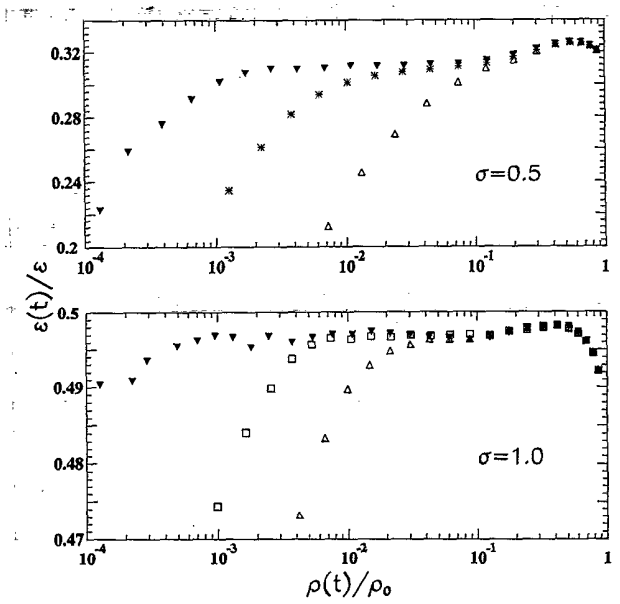

FIG. 5. The ratio of the measured to expected energy density (2.24), up to a constant factor, plotted vs the ratio of measured to initial density of domain walls. The top figure is for $\sigma = 0.5$, while the bottom is for $\sigma = 1.0$. The boundary conditions are periodic. The point types are the same as the previous two figures.

dimensionless combinations of variables:

$$\epsilon(t)/\epsilon = \Phi_E\left[\rho(t)/\rho_0, 1/(\rho(t)L_\infty)\right]. \tag{2.24}$$

In the scaling regime we expect $\Phi_E = \Phi_E[0,0]$ to be constant. We plot $\epsilon(t)/\epsilon$ vs $\rho(t)/\rho_0$ in Fig. 5 for $\sigma = 0.5$ and 1.0, where we calculate the predicted ϵ, up to a constant factor, from the length scale $L(t) = L_\infty/\langle N\rangle$. We use periodic boundary conditions to avoid strong end effects in the energy. The domain walls interact with an infinite-ranged force law so that *all* images of a domain wall around the periodic system are seen (see the Appendix). Note that only 21 runs are done for the largest $\sigma = 1.0$ system. We see the expected early-time transient independent of system size, an intermediate scaling regime growing with system size, and a small-number late-time regime. The energy density for $\sigma = 1.5$ is dominated by the core energy and is simply proportional to the number of domain walls.

While the growth laws agree with the scaling predictions, to investigate scaling we must consider the scaling of the correlation functions directly. If scaling holds, the "energy-scaling" argument determines the growth laws, but the growth laws are not sufficient to determine scaling. To study correlations, we use periodic boundary conditions with infinite-ranged forces. We also use initial conditions randomly chosen from the $\sigma \to \infty$ fixed-point distribution [see Eq. (3.9)], which reduces the initial transients for all σ investigated. We generally use $\Delta t = t/20$, and average over at least 10 000 independent runs, but we present some data at small scaled distances with a finer time step, $\Delta t = t/80$, where we average over 1000 runs.

We first plot the scaled number distribution of domain sizes, $F_L(l/L) = \langle L n_t(l)/N\rangle$, against the scaled domain size, $x = l/L$, in Fig. 6. The exact result for $\sigma \to \infty$ is also shown [calculated from Eq. (3.9)]. The straight lines are the fit, for small x, to the power-law behavior from (2.20). The deviation from the power law at very small x is a result of the geometrically increasing time step in the simulations. Domains of size below l_{min} (2.22) tend to be uniformly distributed. The filled points have four times as many updates per time scale, and are correspondingly closer to the power law. We tabulate the fitted values of β in Table II. The decreasing values of β for decreasing σ indicate stronger shielding and greater correlations between domains.

To obtain the correlation functions, we relate the gradient of the field to the positions of the sharp domain walls:

$$\partial_x \phi(r) = 2\sum_{i=1}^{N} \delta(r - r_i)(-1)^i, \tag{2.25}$$

where the sum is over all domain walls, of alternating sign, at positions $\{r_i\}$. This equation gives the correct discontinuity of the field, $2(-1)^i$, at the domain walls. Similarly, the time derivative of the field is

$$\partial_t \phi(r) = -2\sum_{i=1}^{N} \delta(r - r_i)(-1)^i v_i, \tag{2.26}$$

where v_i is the signed velocity of the domain wall. We then easily calculate

$$C''(r,t) = -\langle \partial_r \phi(r+r_0)\partial_{r_0}\phi(r_0)\rangle_{r_0}$$
$$= -4L_\infty^{-1}\int dr_0 \sum_{ij}(-1)^{i+j}\delta(r+r_0-r_i)\delta(r_0-r_j)$$
$$= L^{-2}\left[-4\delta(x) - 2N^{-1}\sum_{i\neq j}(-1)^{i+j}\{\delta(x-|x_{ij}|)+\delta(x+|x_{ij}|)\}\right] \quad (2.27)$$

and

$$T(r,t) = \langle \partial_t \phi(r+r_0)\partial_t\phi(r_0)\rangle_{r_0}$$
$$= 4L_\infty^{-1}\int dr_0 \sum_{ij}(-1)^{i+j}v_i v_j \delta(r+r_0-r_i)\delta(r_0-r_j)$$
$$= (\dot{L}/L)^2\left[4\langle v^2\rangle \dot{L}^{-2}\delta(x) + 2N^{-1}\sum_{i\neq j}(-1)^{i+j}v_i v_j \dot{L}^{-2}\{\delta(x-|x_{ij}|)+\delta(x+|x_{ij}|)\}\right], \quad (2.28)$$

where $x = r/L$, $x_{ij} = (r_j - r_i)/L$, $L_\infty = NL(t)$, and $\langle v^2\rangle$ is the average square velocity of a domain wall. The real-space scaling forms are

$$C''(r,t) = L^{-2} f''(r/L(t)), \quad (2.29)$$

$$T(r,t) = (\dot{L}/L)^2 b(r/L), \quad (2.30)$$

where the scaling functions $f''(x)$ and $b(x)$ are time independent if scaling holds. We plot $f''(x)$ in the top row and $b(x)$ in the bottom row of Fig. 7 for $\sigma = 0.5$, 1.0, and 1.5. Shown are two times differing by a factor of 4, both chosen from the scaling region of the scaling function Φ (2.23). There are no discernable scaling violations. The solid curves through the data are parameterless estimates assuming independently collapsing domains, which should be valid for small $x > 0$:

$$f''(x) \approx 2N^{-1}\sum_{\langle ij\rangle}\delta(x-|x_{ij}|)$$
$$= 4F_L(x) \quad (2.31)$$

and

$$b(x) \approx 2N^{-1}\sum_{\langle ij\rangle}[v_{ij}/\dot{L}]^2\delta(x-|x_{ij}|)$$
$$\approx 4[v(xL)/\dot{L}]^2 F_L(x)$$
$$\approx 4\beta^2[\Phi^*(\sigma)]^{2(1+\sigma)}(1+\sigma)^2 x^{-2\sigma}F_L(x), \quad x \ll 1 \quad (2.32)$$

where the sum is over neighboring domain walls, $\Phi^*(\sigma)$ is measured from Fig. 3, and $F_L(x)$ is taken from Fig. 6. Following Eq. (2.19), we have used $v(l) = \beta l^{-\sigma}$ with β from Table II. We have also used the scaling amplitude of the growth law, $L(t) = t^{1/(1+\sigma)}/\Phi^*(\sigma)$. For $f''(x)$, the estimate (2.31), assuming independently collapsing domains, is excellent at small x. For $b(x)$, the estimate (2.32) agrees at very small x. An intermediate regime,

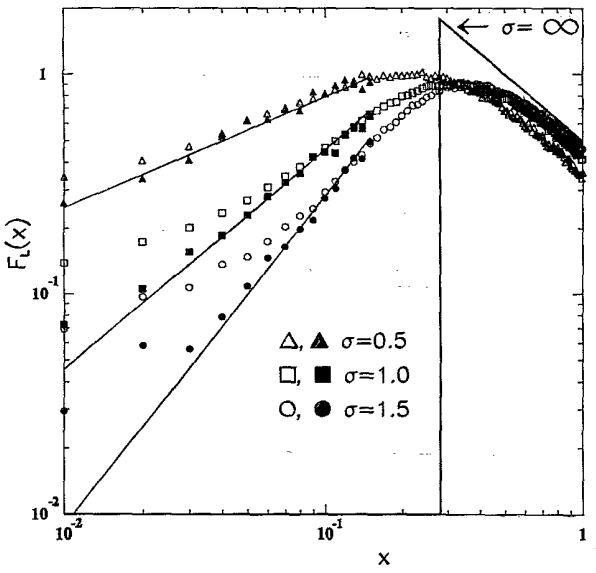

FIG. 6. The distribution of domain sizes, $F_L(x) = Ln_t(xL)/N$, as a function of scaled domain size, $x = l/L(t)$. Note that we have scaled with respect to the *average* domain size $L(t)$. The triangles, squares, and circles correspond to $\sigma = 0.5$, 1.0, and 1.5, respectively. The filled points correspond to simulations with four times as many updates per factor of 2 in time. The line in the upper right is the *exact* result for $\sigma \to \infty$. The straight lines indicate power-law fits for small x [see Eq. (2.20)], as expected for a uniform rate of domain annihilation.

TABLE II. The coefficient of the velocity of fast-moving domain walls, $v(l) \equiv \beta l^{-\sigma}$ for $l \ll L$, obtained by fitting Fig. 6 by the distribution in Eq. (2.20). For $\sigma \to \infty$, the domains are uncorrelated and $\beta = 1$ (see Sec. III).

σ	$\beta(\sigma)$
0.5	0.75 ± 0.05
1.0	0.90 ± 0.05
1.5	0.95 ± 0.05
∞	1

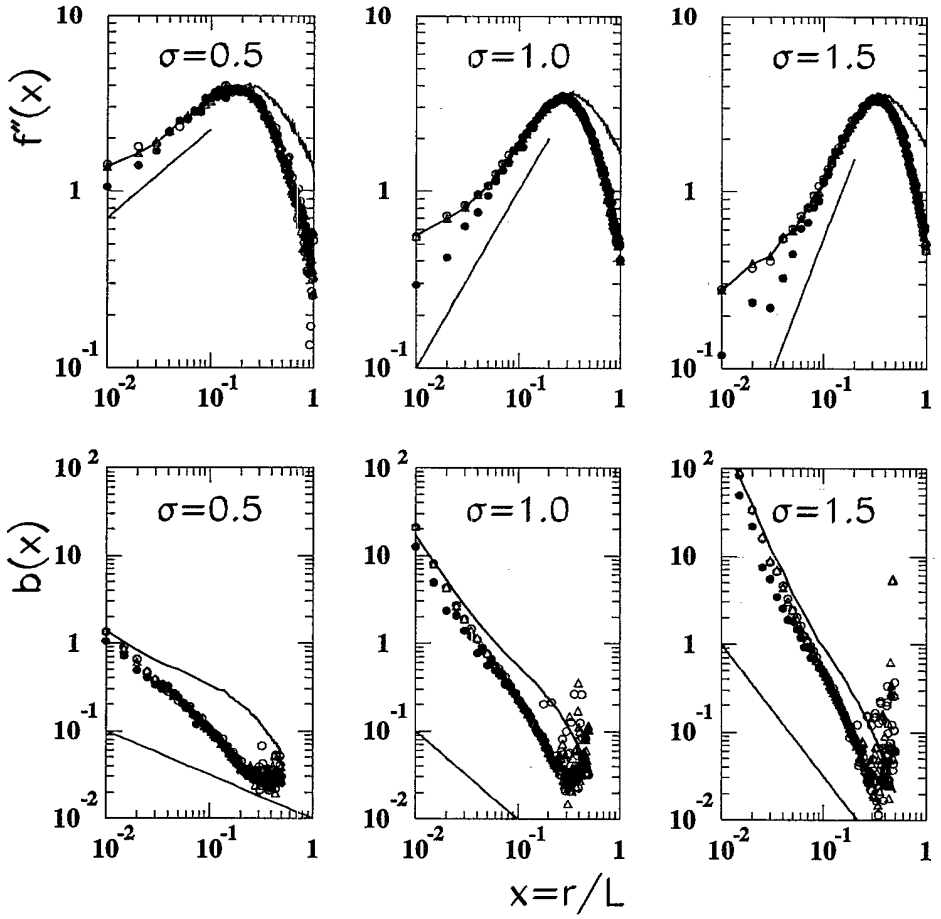

FIG. 7. Real-space correlations plotted against $x = r/L(t)$. The top three figures are the scaled equal-time correlations $f''(x) = L^2C''(r,t)$ for $\sigma = 0.5$, 1.0, and 1.5, while the bottom three figures are the corresponding scaled time-derivative correlations $b(x) = (L/\dot{L})^2T(r,t)$. The open circles correspond to correlations at elapsed times greater by a factor of 4 compared to triangles. The solid lines are described in the text: the upper curve represents a parameterless estimate of the correlations, while the offset straight line represents the expected asymptotic power law for small x. Deviations from the asymptotic power law at $x \ll 1$ are due to the growing time step used — the filled circles correspond to simulations with a finer time step. The error bars have been suppressed for clarity and no data are shown for $b(x)$ with $x > 1/2$.

which grows with decreasing σ, deviates from the estimate and indicates growing correlations between domain-wall velocities in different domains. For $\Delta t/t \to 0$, $f''(x)$ and $b(x)$ should follow the power laws indicated by the offset straight lines, corresponding to $F_L(x) \sim x^\sigma$ for $x \ll 1$ (see Fig. 6). This is evident for $f''(x)$ with the data for $\Delta t/t = 1/80$. For $b(x)$, the regime of independently collapsing domains, where (2.32) holds, probes domain scales of our simulations where $F_L(x)$ does not have its asymptotic small-x behavior [see Eq. (2.22)]. Hence, we do not observe the regime where $g(x)$ exhibits its asymptotic power-law behavior.

We have not shown the $4\langle v^2\rangle \dot{L}^{-2}\delta(x)$ contribution to $b(x)$. From Eq. (2.21), we see that this *breaks* scaling at $r/L = 0$ for $\sigma \geq 1$ due to small rapidly annihilating domains (see also Fig. 2). Hence $T(k,t)$ has a constant contribution that breaks scaling for *all* k for $\sigma \geq 1$. However, this does not change our "energy-scaling" argument, which depends, through $\epsilon_{\rm int}$, only on domains of the characteristic size.

III. SHORT-RANGE INTERACTIONS: CONTINUOUS SPIN MODEL

For systems with only short-range interactions, the domain-wall profiles lead to interactions between adjacent domain walls which drive the phase ordering. From the dynamical Eq. (1.4), the equilibrium profile of an isolated domain wall is determined by $d^2\phi/dx^2 = 4\phi(\phi^2-1)$ — which gives an exponential tail to the domain-wall profile far from the domain wall. The domain walls, treated as particles, are attracted by a corresponding exponential interaction $V(r) = V_0 e^{-|r|/\xi}$, where ξ is the effective width of the domain wall [3], and a resulting pairwise force $F(r) = -dV/dr = V_0\xi^{-1}e^{-|r|/\xi}$. The domain-wall velocities are then simply proportional to their net force. This case has been studied numerically [9], and has been solved by Nagai and Kawasaki [11], who only kept correlations between domains during the rapid domain annihilation process. We rederive their results using a simpler approach [24], which includes the essential correlations of domain annihilation within the approximation of an *instantaneous* domain deletion process. We show that instantaneous annihilation maintains an uncorrelated distribution of domain sizes, approaches a fixed-point solution, and agrees with the real dynamics at late times. This means that the solution of Nagai and Kawasaki is asymptotically exact. Their solution also applies to systems with long-range interactions in the limit $\sigma \to \infty$.

For systems with short-range interactions, or for long-range interactions with $\sigma \to \infty$, the shortest domain collapses instantaneously with respect to longer domains as the average length scale, and hence the typical size difference, grows without bound. When a domain annihilates, the two adjacent domains combine into one large domain which is the size of the original three domains put to-

gether (see Fig. 8). The three domain sizes are strongly correlated during the rapid annihilation process, but only one domain is left at the end, uncorrelated with *its* neighbors.

We consider a system with no initial correlations between domain sizes, and consider a set containing all of the domain lengths. The instantaneous collapse of the shortest domain corresponds to taking the smallest length from the set of domain lengths, adding it to two lengths randomly chosen from the set (which is equivalent to the lengths of two uncorrelated neighbors), and replacing the three lengths by one length equal to their sum. As this procedure is iterated, the distribution of domain sizes, scaled by the size of the smallest domain, $\tilde{L}(t)$, will approach a fixed-point distribution. There will be no correlations formed between the lengths of different domains because the collapse of the shortest domain forms a single domain with its neighbors independently of the other domains in the system. This is similar, in that respect, to the "paste-all" model of Derrida *et al.* [24]. Since all higher-point correlations are zero, the domain-size distribution function describes the fixed point of this "instantaneous-collapse" model.

If $n_t(l)\delta l$ is the number of domains of sizes in the interval $[l, l+\delta l]$ in the entire system, then

$$N(t) = \int_{\tilde{L}}^{\infty} n_t(l)dl, \tag{3.1}$$

$$L_\infty = \int_{\tilde{L}}^{\infty} l n_t(l)dl, \tag{3.2}$$

$$f_t(l) = n_t(l)/N(t), \tag{3.3}$$

$$F(l/\tilde{L}, t) = \tilde{L} f_t(l), \tag{3.4}$$

where $N(t)$ is the number of domains in the system, L_∞ is the length of the system, $f_t(l)$ is the probability density of domain sizes, and $F(x,t)$ is the scaled probability density with respect to the minimum domain size $\tilde{L}$. Note that $n_t(l)$ is the same as used in Sec. II A. We will determine the time-independent fixed-point distribution $F(x)$.

Each domain that annihilates combines with the two adjacent domains, each of length l with probability density $f_t(l)$. Conversely, for each domain that annihilates, one large domain is formed at length l with a probability density coming from two domains combining, one of length l' and the other of length $l-l'-\tilde{L}$, both restricted to be larger than $\tilde{L}$. In a time interval δt, the minimum length will shift by $\delta\tilde{L} = \tilde{L}(t+\delta t) - \tilde{L}(t)$, and $n_t(\tilde{L})\delta\tilde{L}$ domains will annihilate. This leads to an evolution equation for the number distribution $n_t(l)$:

$$n_{t+\delta t}(l) = n_t(l) + n_t(\tilde{L})\delta\tilde{L} \times\left[-2f_t(l) + \int_{\tilde{L}}^{\infty} dl' f_t(l') f_t(l-l'-\tilde{L}) \times\Theta(l-l'-2\tilde{L})\right]. \tag{3.5}$$

The evolution equation for the scaled probability density $F(x,t)$ follows:

$$\tilde{L}dF(x,t)/d\tilde{L} = F(x,t) + xdF(x,t)/dx + F(1,t)\int_1^{\infty} dx' F(x',t)F(x-x'-1,t) \times\Theta(x-x'-2). \tag{3.6}$$

Using the Laplace transform, $\phi(p,t) = \int_1^{\infty} dx e^{-px} F(x,t)$, we obtain

$$\tilde{L}d\phi/d\tilde{L} = -pd\phi/dp + F(1,t)e^{-p}\left[\phi^2 - 1\right]. \tag{3.7}$$

For the stationary solution we set $d\phi/d\tilde{L} = 0$, use $\phi(0) = 1$, and force consistency on $d\phi/dp|_{p=0}$ to determine $F(1) = 1/2$ [25]. Hence the stationary solution to (3.7) is

$$\phi(p) = \tanh\left[E_1(p)/2\right], \tag{3.8}$$

where $E_1(p) = \int_p^{\infty} dx e^{-x}/x$. This agrees with Nagai and Kawasaki [11]. Expanding the tanh and doing the inverse transform leads to a scaling fixed-point distribution

$$F(x) = \sum_{i=0}^{[(x-1)/2]} A_{2i+1} \int_1^{\infty} \prod_{j=1}^{2i+1} \frac{dx_j}{x_j} \delta\left(x - \sum x_j\right), \quad x \geq 1 \tag{3.9}$$

where the first sum is for all i such that $x \geq 2i+1$, and $2^n A_n$ are the Taylor expansion coefficients of $\tanh(x)$. The fixed-point distribution is piecewise analytic, with discontinuities at $x = 2i+1$ in the $2i$th derivative for all integer $i \geq 0$. The fixed-point distribution is simple for small x:

$$F(x) = \begin{cases} 0, & x \in [0,1) \\ 1/(2x), & x \in [1,3] \end{cases} \tag{3.10}$$

but gets progressively more complicated in every succeeding interval of width 2.

The growth law of the average domain size, $L(t) = L_\infty/N(t)$, is derived by matching the flux of annihilating domains $j(\xi)$ to the flux of domains coming from the minimal domain size $\tilde{L}$. From the discussion lead-

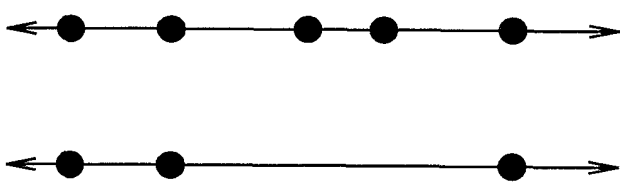

FIG. 8. For systems with short-range interactions, or with long-range interactions where $\sigma \to \infty$, the smallest domain will annihilate instantaneously with respect to larger domains. A single large domain is formed of size equal to the smallest domain and its two neighbors. The filled circles indicate domain walls.

ing to Eq. (2.20), the flux of annihilating domains is given by $j(\xi) = \dot{N}/2 = -\dot{L}N/(2L)$. For systems with short-range interactions, the flux at $\tilde{L}$ is given by $j(\tilde{L}) = -(N/\tilde{L})e^{-\tilde{L}/\xi}$, where $n_t(\tilde{L}) = (N/\tilde{L})F(1)$ is the number density of domains at scale $\tilde{L}$, they are collapsing at a rate $-2e^{-\tilde{L}/\xi}$ (twice the speed of each end), and $F(1) = 1/2$. Equating these fluxes gives a logarithmic growth law

$$\tilde{L} = \xi \ln(t/t_0), \tag{3.11}$$

where t_0 depends on the form of the potential $V(\phi)$.

For systems with long-range interactions, with $\sigma \to \infty$, we can also obtain the exact growth law. The flux of annihilating domains is again given by $j(\xi) = -\dot{L}N/(2L)$. The flux at $\tilde{L}$ is now given by $j(\tilde{L}) = -N/\tilde{L}\tilde{L}^{\sigma}$, where the domains of scale $\tilde{L}$ are collapsing at a rate $-2\tilde{L}^{-\sigma}$. Equating these fluxes gives $d\tilde{L}/dt = 2\tilde{L}^{-\sigma}$, and so $L(t) = 2e^{\gamma_E}t^{1/(1+\sigma)}$ in the $\sigma \to \infty$ limit. This determines the scaling amplitude in that limit:

$$\Phi^*(\infty) = g_R^*(\infty) = e^{-\gamma_E}/2 \simeq 0.28, \tag{3.12}$$

where the fixed-point amplitude used by Lee and Cardy is $g_R^*(\sigma) = \Phi^*(\sigma)[2(1+\sigma)]^{1/(1+\sigma)}$ [8]. This exact result is comparable to the perturbative calculation by Lee and Cardy, who found $g_R^*(\infty) \approx 0.33$.

The average domain size is given by

$$\begin{aligned} L(t) &= \tilde{L}\int_1^\infty xF(x)dx \\ &= -\tilde{L}d\phi/dp|_{p=0} \\ &= \tilde{L}2e^{\gamma_E}, \end{aligned} \tag{3.13}$$

where we have used the asymptotic form of (3.8), and $\gamma_E \simeq 0.577$ is the Euler constant. This agrees with Nagai and Kawasaki [11] and numerical results [9].

The scaled distribution of domain sizes, $F_L(x) = Ln_t(xL)/N$, is plotted against the scaled domain size, $x = l/L(t)$, for $\sigma = 0.5$, 1.0, and 1.5 in Fig. 6. The exact result for $\sigma \to \infty$ is also shown. As σ increases, the distribution approaches the $\sigma \to \infty$ fixed-point distribution.

The structure function is calculated by Kawasaki *et al.* [12] from the Fourier transform of (2.27) and the domain-size distribution function:

$$S(k) = \frac{4}{k^2L}\frac{1 - |\tanh[E_1(ik\tilde{L})/2]|^2}{|1 + \tanh[E_1(ik\tilde{L})/2]|^2}, \tag{3.14}$$

which, because $L/\tilde{L}$ is constant, satisfies the scaling form (2.8).

Since domains annihilate independently and only adjacent domain walls have correlated velocities, the real-space time-derivative correlation function (2.28) is simplified:

$$\begin{aligned} T_{\rm SR}(r,t) &= (\dot{L}/L)^2\left\{4\langle v^2\rangle\dot{L}^{-2}\delta(x) + 4N^{-1}\sum_{\langle ij\rangle}(-1)^{i+j}v_iv_j\dot{L}^{-2}\delta(|x| - |x_{ij}|)\right\} \\ &\simeq (\dot{L}/L)^2\{4\langle v^2\rangle\dot{L}^{-2}\delta(x) + 4F_L(|x|)[v(|x|L)/\dot{L}]^2\}, \end{aligned} \tag{3.15}$$

where $x = r/L$, $F_L(x)$ is the domain distribution function scaled with respect to the average domain size L, and $\langle v^2\rangle$ is the average square velocity of a domain wall. The equation becomes exact, though the scaling behavior is unchanged, if we use the root-mean-square velocity of a wall of a domain of size l in the second line rather than $v(l)$. For both short-range and $\sigma \to \infty$ systems, the average square velocity is dominated by the tiny flux of annihilating domains. Following Eq. (2.21), the average square velocity will be

$$\langle v^2\rangle \sim \dot{L}L^{-1}\int_\xi^L dl\, v(l). \tag{3.16}$$

The integral diverges at small l for both short-range systems and long-range systems with $\sigma > 1$, and the square velocity is dominated by small annihilating domains, $\langle v^2\rangle \sim \dot{L}/L$. Hence the scaling (2.10) of the time-derivative correlations (3.15) is broken at $x = 0$. The scaling for $x > 0$ holds if $v(xL)/\dot{L}$ is time independent. For long-range interactions, with $v(l) \sim l^{-\sigma}$ and $\dot{L} \sim L^{-\sigma}$, this is true and the $T(r,t)$ scales for $r/L > 0$. For short-range interactions, $v(l) \sim e^{-l/\xi}$. Since $\tilde{L} = \xi\ln(t/t_0)$, (3.11), scaling only holds at $x = \tilde{L}/L \simeq 0.28$, and is broken at all other x.

There will be small correlations between the sizes of different domains because the suppression of the motion of domain walls relative to those of the smallest domain is not complete. The strongest of these effects is the slow evolution of adjacent domain walls in any given domain of size $L_i > \tilde{L}$. The strength of this evolution is characterized by the fractional length change $\Delta L_i/L_i$ of the domain before it is annihilated or combines with another domain. We overestimate ΔL_i by neglecting combination events and integrating the length change until the domain is of the scale of the shortest domain (where it must annihilate):

$$\Delta L_i \simeq \int_{\tilde{L}}^{L_i} d\tilde{L}'R(\tilde{L}'), \tag{3.17}$$

where R is the ratio of the average force on a domain wall to the evolution rate of the minimum domain size, $d\tilde{L}/dt$. We also neglect the direct force between adjacent domain walls in comparison to the contribution of shorter adjacent domains to R. For short-range forces,

$$\begin{aligned} R &\simeq \int_1^\infty dxF(x)e^{-\tilde{L}x/\xi}/(2e^{-\tilde{L}/\xi}) \\ &\simeq e^{\tilde{L}/\xi}\int_1^\infty \frac{dx}{4x}e^{-\tilde{L}x/\xi} \\ &\simeq \xi/(4\tilde{L}), \end{aligned} \tag{3.18}$$

where $F(x)$ is the fixed-point distribution of the scaled domain size (3.9). Hence

$$\Delta L_i/L_i \sim (\xi/L_i)\ln(L_i/\tilde{L}), \tag{3.19}$$

and the effect of the slow drift vanishes at late times as $L \to \infty$. For long-range forces, the same calculation leads to

$$\begin{aligned} R &\simeq \int_1^\infty dx F(x)(\tilde{L}x)^{-\sigma}/(2\tilde{L}^{-\sigma}) \\ &\simeq \int_1^\infty \frac{dx}{4x}x^{-\sigma} \\ &= 1/(4\sigma). \end{aligned} \tag{3.20}$$

Hence the fractional change due to the slow drift is given by

$$\Delta L_i/L_i \sim \sigma^{-1}(1-\tilde{L}/L_i), \tag{3.21}$$

and vanishes in the limit $\sigma \to \infty$. Hence as $\tilde{L}/\xi \to \infty$ or $\sigma \to \infty$, the slow evolution of adjacent domain walls in domains larger than the minimum size can be neglected. For power-law interactions, the scale of the cumulative effect of interactions between domain walls at larger distances, $r > 2\tilde{L}$, is smaller by a factor of $\sum_{n=2}^\infty n^{-\sigma}$ and also vanishes as $\sigma \to \infty$.

We see that our "instantaneous-deletion" model agrees with the evolution of a real system in the limit as $t \to \infty$, and so has the same fixed-point solution that we have exactly determined. Any initial long-range correlations between domain sizes will necessitate a more complex treatment (see, e.g., [26]), though we expect any short-range correlations to vanish as the system coarsens.

IV. CONCLUSIONS

From the energetics of scaling 1D scalar systems, we predict growth laws $L(t) \sim t^{1/(1+\sigma)}$ for all $\sigma > 0$. This growth law is of the same form as the length scale given by a collapsing isolated domain (2.2). The intuitive picture is of collapsing domains leaving "voids" which set the growing length scale. These growth laws agree with previous predictions for $0 < \sigma < 1$ [4,7]. We confirm our predicted growth laws, with simulations for $\sigma = 0.5$, 1.0, and 1.5—one value in each of the three regimes of the equilibrium system. Different boundary conditions and system sizes only affect the late-time, small-number regime of our simulations, and so the thermodynamic limit is well behaved. The anomalous growth law seen by Lee and Cardy [8] for $\sigma = 0.5$ was the result of large finite-size effects—a scaling regime appears for larger systems than they considered. The nonanalyticities seen by Lee and Cardy [8] for $0 < \sigma \leq 1$ must be controlled in an infinite system with a fixed initial density. We find that the equal-time and time-derivative correlations scale for $r/L > 0$ at $\sigma = 0.5$, 1.0, and 1.5. For $r \ll L$, correlations can be well approximated by assuming that domains collapse independently. This approximation becomes better with increasing σ. For $\sigma \geq 1$, scaling of the time-derivative correlations does not hold at $r/L = 0$ due to small rapidly annihilating domains.

For purely short-range interactions, and for long-range interactions in the $\sigma \to \infty$ limit, we show that the solution by Nagai and Kawasaki [11] of the domain-size distribution, which assumes uncorrelated domain sizes, is exact. Hence their expression for the structure factor (3.14), which satisfies scaling, is also exact. We determine the time-derivative correlation function, which *breaks* scaling at core scales, and more generally for systems with purely short-range interactions. For systems with long-range interactions described by (2.2) and (2.3), we determine the exact growth law amplitude in the $\sigma \to \infty$ limit, $L(t) = t^{1/(1+\sigma)}/g_R^*(\infty)$ with $g_R^*(\infty) = e^{-\gamma_E}/2 \simeq 0.28$.

ACKNOWLEDGMENT

We thank T. Blum, J. Cardy, and B. P. Lee for discussions.

APPENDIX: RESUMMING DOMAIN-WALL INTERACTIONS IN A PERIODIC SYSTEM

With long-range forces in a periodic system, each domain wall interacts with an infinite number of images of each other domain wall. Using the interaction (2.2), the total force between two domain walls is given by

$$\begin{aligned} f(l) &= -l^{-\sigma} + \sum_{n=1}^\infty \left[(nL_\infty - l)^{-\sigma} - (nL_\infty + l)^{-\sigma}\right] \\ &= -l^{-\sigma} + \sum_{n=1}^\infty [\Gamma(\sigma)]^{-1} \int_0^\infty dt t^{\sigma-1}[e^{-(nL_\infty - l)t} - e^{-(nL_\infty + l)t}] \\ &= -l^{-\sigma} + \frac{L_\infty^{-\sigma}}{\Gamma(\sigma)} \int_0^\infty dx x^{\sigma-1} \frac{\sinh[l/(xL_\infty)]}{\sinh[x/2]} e^{-x/2}, \end{aligned} \tag{A1}$$

where l is the closest distance between the domain walls around the loop and L_∞ is the system size. The force is attractive along their nearest separation if the domain walls are of opposite sign and repulsive if of the same sign. The interaction energy can be similarly calculated using (2.1):

$$E(l) - E(L_\infty) = l^{1-\sigma} + \frac{L_\infty^{1-\sigma}}{\Gamma(\sigma-1)} \int_0^\infty dx x^{\sigma-2} \left[\frac{\cosh(lx/L_\infty) - 1}{\sinh(x/2)}\right] e^{-x/2}, \qquad \sigma \neq 1 \tag{A2}$$

where we have adsorbed a factor of $(\sigma-1)^{-1}$. An overall -1 factor is introduced between domain walls of opposite sign. For $\sigma \neq 1$ the integrals are done numerically and stored in lookup tables for use in the simulations. For $\sigma = 1$, the integrals can be done exactly:

$$f_{\sigma=1}(l) = -\pi L_\infty^{-1} / \tan(\pi l / L_\infty), \tag{A3}$$

$$E_{\sigma=1}(l) - E_{\sigma=1}(L_\infty) = \ln l + \ln\left[\frac{\sin(\pi l/L_\infty)}{\pi l/L_\infty}\right]. \tag{A4}$$

[1] See, e.g., J. D. Gunton, M. San Miguel, and P. S. Sahni, in *Phase Transitions and Critical Phenomena*, edited by C. Domb and J. L. Lebowitz (Academic, New York, 1983), Vol. 8, p. 267; J. S. Langer, in *Solids Far From Equilibrium*, edited by C. Godrèche (Cambridge, Cambridge, MA, 1992); A. J. Bray, in *Phase Transitions in Systems with Competing Energy Scales*, edited by T. Riste and D. Sherrington (Kluwer Academic, Boston, 1993); H. Toyoki, in *Formation, Dynamics and Statistics of Patterns*, edited by K. Kawasaki, M. Suzuki, and A. Onuki (World Scientific, Singapore, 1994), Vol. 2.

[2] S. M. Allen and J. W. Cahn, Acta Metall. **27**, 1085 (1979).

[3] K. Kawasaki and T. Ohta, Physica A **116**, 573 (1982).

[4] A. J. Bray, Phys. Rev. E **47**, 3191 (1993).

[5] H. Hayakawa, Z. Rácz, and T. Tsuzuki, Phys. Rev. E **47**, 1499 (1993); T. Ohta and H. Hayakawa, Physica A **204**, 482 (1994).

[6] H. Hayakawa, T. Ishihara, K. Kawanishi, and T. S. Kobayakawa, Phys. Rev. E **48**, 4257 (1993); J. A. N. Filipe and A. J. Bray (unpublished).

[7] A. J. Bray and A. D. Rutenberg, Phys. Rev. E **49**, 27 (1994); A. D. Rutenberg and A. J. Bray (unpublished).

[8] B. P. Lee and J. L. Cardy, Phys. Rev. E **48**, 2452 (1993).

[9] T. Nagai and K. Kawasaki, Physica A **120**, 587 (1983); F. de Pasquale, P. Tartaglia, and P. Tombesi, Phys. Rev. A **31**, 2447 (1985).

[10] H. Ikeda, J. Phys. C **16**, 3563 (1983); **19**, L535 (1986); N. Metoki, H. Suematsu, Y. Murakami, Y. Ohishi, and Y. Fujii, Phys. Rev. Lett. **64**, 657 (1990).

[11] T. Nagai and K. Kawasaki, Physica A **134**, 483 (1986).

[12] K. Kawasaki, A. Ogawa, and T. Nagai, Physica B **149**, 97 (1988).

[13] Exotic potentials with nonquadratic or asymmetric minima will lead to different phase-ordering behavior in 1D systems with short-range interactions since the growth is not curvature driven.

[14] P. C. Hohenberg and B. I. Halperin, Rev. Mod. Phys. **49**, 435 (1977).

[15] F. J. Dyson, Commun. Math. Phys. **12**, 91 (1969); **12**, 212 (1969); J. M. Kosterlitz, Phys. Rev. Lett. **37**, 1577 (1976); J. K. Bhattacharjee, J. L. Cardy, and D. J. Scalapino, Phys. Rev. B **25**, 1681 (1982).

[16] A. J. Bray, Phys. Rev. Lett. **62**, 2841 (1989); Phys. Rev. B **41**, 6724 (1990); T. J. Newman and A. J. Bray, J. Phys. A **23**, 4491 (1990). Note that the temperature dependence of the $\sigma = 1$ case, with a line of equilibrium fixed points at low temperatures [15], has not been studied.

[17] J. G. Amar and F. Family, Phys. Rev. A **41**, 3258 (1990); A. J. Bray, J. Phys. A **22**, L67 (1990).

[18] We assume a velocity-independent wall mobility, so that velocities are proportional to the force. This is explicitly shown for $0 < \sigma \leq 1$, at low temperatures with no domain creation, by Lee and Cardy [8].

[19] H. Furukawa, Adv. Phys. **34**, 703 (1985).

[20] G. Porod, in *Small-Angle X-Ray Scattering*, edited by O. Glatter and O. Kratsky (Academic, New York, 1982); P. Debye, H. R. Anderson, and H. Brumberger, J. Appl. Phys. **28**, 679 (1957); Y. Oono and S. Puri, Mod. Phys. Lett. B **2**, 861 (1988).

[21] Our simulations are done with systems of a fixed initial density and various lengths. This proved most convenient for choosing the time scales of simulations. Different initial densities can be formally mapped to a fixed density with a change of time scale and system size without changing the scaling functions.

[22] The distribution of domains with sizes $l \lesssim l_{\min}$ is changed (made more uniform) by a geometrically increasing time step. This affects short-distance correlations.

[23] Free boundary conditions for the domains, which are used, have half-strength domain walls at the end of the system and net "charge neutrality" of the signed domain walls.

[24] B. Derrida, C. Godrèche, and I. Yekutieli, Phys. Rev. A **44**, 6241 (1991); see also A. J. Bray, B. Derrida, and C. Godrèche, Europhys. Lett. **27**, 175 (1994).

[25] We ignore cases where the average domain size $L(t)$ is infinite. From the small-p asymptotics of the solution, $\phi \simeq 1 - O(p^{2F(1)})$, these cases correspond to $F(1) < 1/2$ so that $-d\phi/dp|_{p=0}$, which gives the first moment of $F(x)$, is infinite. Cases with $F(1) > 1/2$ are unphysical — they correspond to a vanishing average domain size [see Eq. (3.13)].

[26] K. Kawasaki and T. Nagai, Physica A **121**, 175 (1983).